NANO LETTERS

2007
Vol. 7, No. 1
116−119

Using Gold Nanorods to Probe Cell-Induced Collagen Deformation

John W. Stone,[†] Patrick N. Sisco,[†] Edie C. Goldsmith,[‡] Sarah C. Baxter,[§] and Catherine J. Murphy*,[†]

Department of Chemistry and Biochemistry and Department of Mechanical Engineering, University of South Carolina, Columbia, South Carolina 29208, and Department of Cell and Developmental Biology and Anatomy, University of South Carolina School of Medicine, Columbia, South Carolina 29208

Received September 23, 2006; Revised Manuscript Received November 19, 2006

ABSTRACT

In biological tissue, complex mechanisms of cellular response are closely linked to the mechanical environment that cells experience. The key to understanding these mechanisms may lie in measurement of local mechanical fields near living cells and between cells. We have developed a novel optical measurement technique which combines the light elastically scattered from gold nanorods with digital image analysis to track local deformations that occur in vitro between cells, in real time, under darkfield optical microscopy. We find that measurable tension and compression exist in the intercellular matrix at the length scale of micrometers, as the cells assess, adapt, and rearrange their environment.

It is well-established that cellular response to mechanical environment is critical to cell/tissue function.[1−8] Studies have shown that physical cues, transmitted through the largely collagenous network of the extracellular matrix (ECM), are recognized by the cells and trigger complex mechanical and biochemical responses (mechanotransduction) including adaptive remodeling.[1−8] Many studies have examined the bulk mechanical response of tissues; others have focused on the properties and response of isolated cells under mechanical load, specifically adaptive changes to the cytoskeleton.[1−9] In vivo, however, it is likely that characterization of the local mechanical environment experienced by cells, on the length scale of micrometers, may be needed to more clearly elucidate the complex mechanisms associated with mechanotransduction.[10]

Metallic nanoparticles that have at least one dimension in the 1−100 nm size regime are gaining increased usage in biological applications due to their small size and unique optical properties in the visible−near-infrared region of the electromagnetic spectrum.[11] Nanoscale metal particles exhibit brilliant colors in the visible region that are due to the collective oscillation of electrons, termed plasmons, in the conduction band of the metal.[11] Furthermore, the position and number of the plasmon bands of a metal can be tailored by rational control of particle size, shape, and aggregation state.[12−15]

In this paper we describe experiments in which gold nanorods are used to track local deformations between cells and within the ECM in real time. Previously, we have shown that this general approach correctly yields local deformation and strain data in manually stretched poly(vinyl alcohol) and poly(dimethylsiloxane) thin films, in which no local heterogeneity was expected.[16] In this work, gold nanorods are embedded in cell-populated (neonatal cardiac fibroblasts) collagen films. Collagen gels or films are widely accepted as a material model for the ECM. The cell−collagen films undergo endogenous loading due to cell traction forces as the cells, through their physical attachments to the ECM network, test their environment. This assessment of the surrounding structure directs cell morphology, can potentially guide cell migration, and can initiate adaptive remodeling of the ECM, including the production of additional collagen.[1] The relatively short term results of this loading, however, are local deformations, as the cells tug on the collagen.

As the collagen network is deformed by cell traction forces, the pattern of scattered light from the embedded nanorods also shifts and deforms. Digital image analysis can then be used to track the movement and deformation of the light pattern and to calculate local material deformations. Simultaneous fluorescence imaging can also be used to identify cell locations, in order to associate strain fields with the relevant cell spatial positions, morphologies, and orientations.

Gold nanorods (376 ± 105 nm long, 26 ± 5 nm wide) were prepared in aqueous solution using a seed-mediated surfactant-directed approach previously described and puri-

* To whom correspondence should be addressed: Murphy@mail.chem.sc.edu.
[†] Department of Chemistry and Biochemistry, University of South Carolina.
[‡] Department of Cell and Developmental Biology and Anatomy, University of South Carolina School of Medicine.
[§] Department of Mechanical Engineering, University of South Carolina.

10.1021/nl062248d CCC: $37.00
Published on Web 12/06/2006

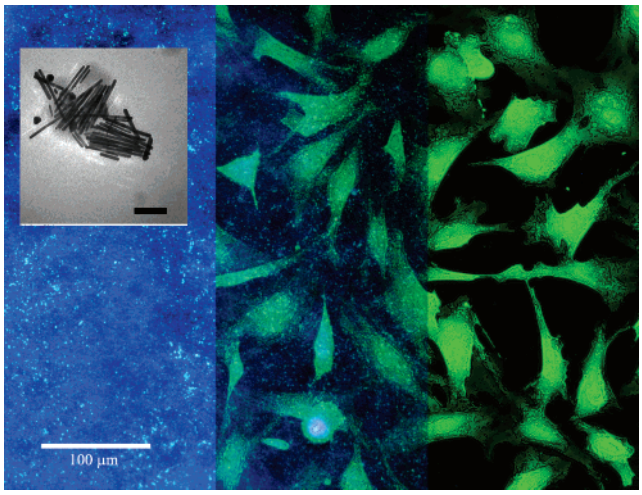

Figure 1. Darkfield optical micrograph of light scattered from gold nanorods (left panel). Simultaneous fluorescence image of cardiac fibroblasts (right panel). The two images superimposed with some transparency (center panel). Fluorescent image has been enhanced by outlining the cells and increasing contrast for clarity in the overlay. Scale bar = 100 μm. Inset: Transmission electron micrograph of the gold nanorods. Scale bar (inset) = 100 nm.

fied by centrifugation and washing.[17−19] The overall reaction is one in which $HAuCl_4$ is reduced to elemental gold in the presence of a cationic surfactant, cetyltrimethylammonium bromide (CTAB). The nanorods are coated with a bilayer of the cationic surfactant CTAB, which renders them water-soluble and highly positively charged.[20,21] We have previously shown that CTAB bound to small gold spheres is not cytotoxic to human cells.[22]

Collagen thin films were prepared by adding 250 μL of a solution containing 100 μL of 0.2 N HEPES buffer (pH 9.0), 100 μL of 10X MEM, and 800 μL of type I collagen to a square chamber slide.[23] The film was cured at approximately 40 °C for >2 h. Subsequently, a second layer was added to the already cured collagen film. To this top layer was added dropwise 25 microliters of nanorod solution. The film was cured again at approximately 40 °C overnight. These films were subsequently plated with 100 000 neonatal rat cardiac fibroblasts and stained with a fluorescent dye, 5-chloromethylfluoresceindiacetate (CMFDA). Once plated, the films were incubated (5% CO_2, 37 °C) for approximately 5 h prior to imaging. All optical studies were performed on a Nikon Eclipse model ME600L microscope equipped with bright field, dark field, and fluorescent imaging capabilities. The excitation wavelength range for the fluorescence imaging was 450−490 nm.

Images were collected over a 2-h time interval between 5 and 7 h after cell plating. This time period allowed for the measurement of cell-induced deformations both locally, around individual cells, and collectively over multiple cell domains. The components of the imaging are shown in the three panels of Figure 1: from left to right, the field of scattered light from the nanorods (darkfield image), with inset showing a transmission electron microscopy (TEM) image of nanorods; an overlay of the nanorods over the cells (darkfield and fluorescence); and the field of cells (fluorescence).

To illustrate the degree of cell extension movement, fluorescence images of the stained cells taken at the beginning and at the end of the time sequence used in this work are shown in Figure 2. Changes in cell morphology and motion of cell extensions are visible. The reader is referred to the Supporting Information for a more clear and compelling visualization of this process.

Many of these visible cell motions will result in a corresponding deformation of the underlying and surrounding collagen network. Since cells attach at discrete points, through focal adhesions, the application of the load may not be uniformly distributed along the outline of the cell and not all cell motion will result in deformation of the collagen. It has also been well-established that at the micrometer scale, the collagen network itself does not behave as a homogeneous material, and its varying stiffness and density will result in spatially different responses under the same loads.[24]

Tracking these locally varying displacement and strain fields was done using the image correlation software VIC-2D, developed at the University of South Carolina.[25] This software maps spatial locations in an undeformed reference state to locations in images taken at various stages of deformation by comparing (correlating through an optimization algorithm) pixel gray scale intensities in a sequence of small subareas of the full digital image. In our case, the spatial locations correspond to the light scattered from gold nanorods at different places in the image, and pixels are either gray (no nanorods in that spot) or white (nanorods are in that spot). As the nanorods move in concert with the collagen in which they are embedded, the positions of the scattered light "pixels" are displaced. Displacements are measured directly from this mapping. The software then constructs a smooth surface through the displacement field and approximates strains, which are gradients of displacements and are dimensionless, by differentiating this surface. The Lagrangian (nonlinear) strains, $\gamma_{ij} = (1/2)((\partial u_i/\partial X_j) + (\partial u_j/\partial X_i) + (\partial u_k/\partial X_i)(\partial u_k/\partial X_j))$ (summed over k), where γ_{ij} are the components of the strain tensor in the plane, $\mathbf{u} = \mathbf{x} - \mathbf{X}$ is the displacement vector, defined as the change between the deformed position $\mathbf{x} = (x_1, x_2, x_3)$ and the reference position $\mathbf{X} = (X_1, X_2, X_3)$ are calculated, which makes the method appropriate for biological materials which are likely to experience large strains; small (linearized) strain theory approximation would be less accurate.

Contour maps of the normal strain in the horizontal (x-axis) direction at the time points 320, 400, and 420 min are shown in Figure 3. The scale of the strain fields in all three images is the same.

By convention, compressive strains are labeled as negative and tensile strains positive. In Figure 3, strains run from a maximum magnitude of compressive strain of 0.0015 (violet) to a maximum tensile strain (red) of 0.0038. Visually, zero strain is the middle (green). Improper focusing might lead to apparent strain fields. Inconsistent focusing might generate apparent strains in addition to the true planar fields. We performed control experiments in which we deliberately focused and unfocused the microscope, and from the resulting "displacements" of the nanorods, calculated strain fields. The

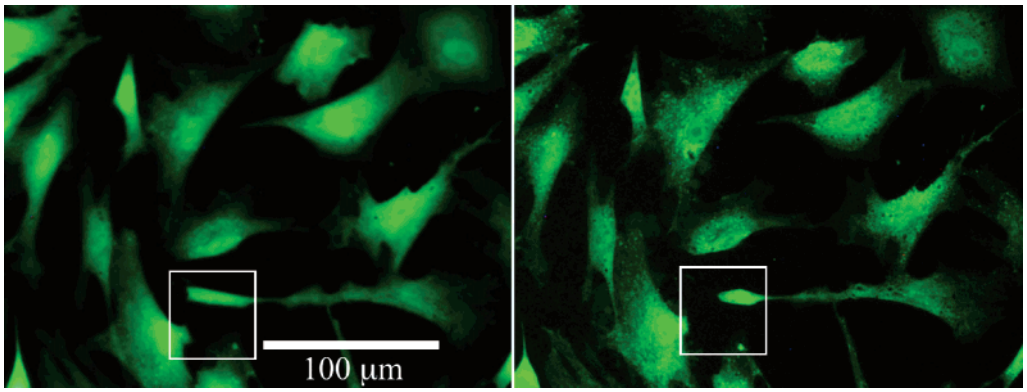

Figure 2. Fluorescence images of stained fibroblast cells at $t = 5$ h (left) and $t = 7$ h (right). Cells show changes in morphology as they mechanically adjust to their environment.

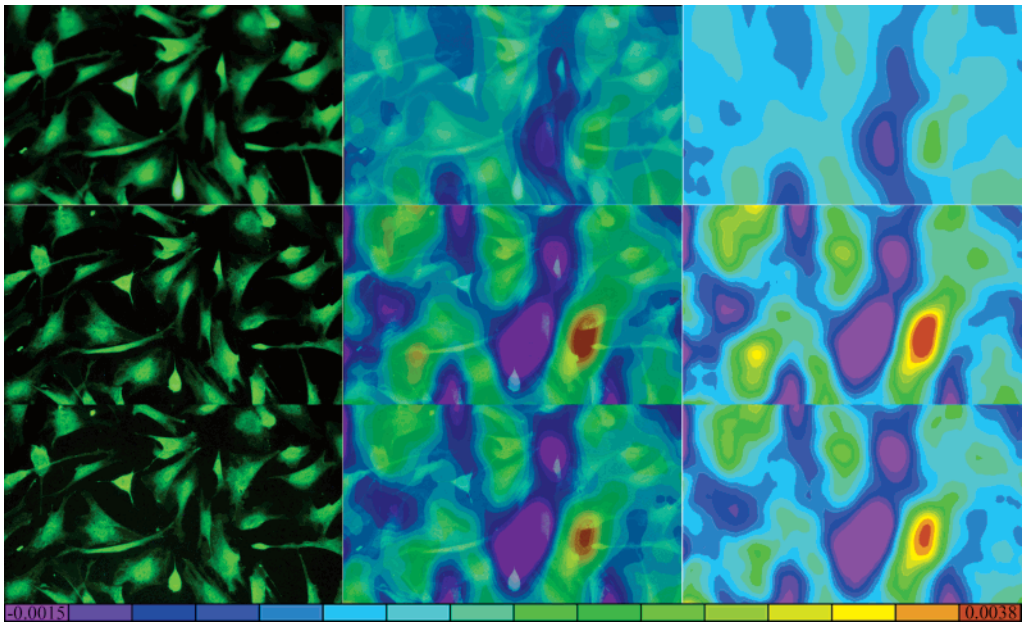

Figure 3. Cells and corresponding strain field maps: row 1, $t = 320$ min; row 2, $t = 400$ min; row 3, $t = 420$ min. In each row, left to right, are the fluorescently tagged cells, a transparent overlay of strain fields on cells, and strain fields. Violet indicates the maximum compressive strain and red the maximum tensile strain. Color scale at the bottom runs from violet −0.0015 (compressive) to 0.0038 (tensile) strain.

strains resulting from refocusing a single image were on the order of 0.00002 (0.002%), far smaller than the strains measured when cells were actually moving.

Under the conditions of these tests, cellular response would be expected to vary with film thickness, collagen concentration, and cell density. These experiments are in progress. However, it is possible to see in the data already presented the progression of tension followed by relaxation corresponding to the movement of the cell extensions. Movies showing the cell motion (as per Figure 2) and the complete set of fields evolving over time for the horizontal strains (as per Figure 3) as well as for the vertical strains, are available as Supporting Information.

A purely qualitative examination based on Figure 3 suggests a visual form of the correlation between the patterns of tensile and compressive strains and the patterns in cell spatial arrangement. Further quantitative analysis can be done using the software to extract data from specific regions for more specific comparisons to cell shape, locations, or orientations, etc. For example, Figure 4 plots axial strains as a function of position along a horizontal line across one region of the digital image (Figure 4 insert). Clearly, at different times, a given region of the cell−collagen composite

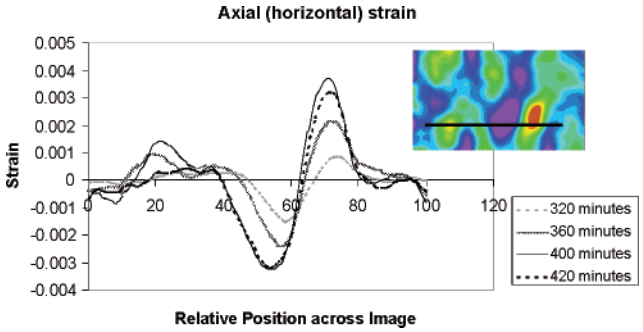

Figure 4. Axial strains as a function of position through one slice of the data (inset) for various times: light dashed line, 320 min; thick solid line, 360 min; thin solid line, 400 min; dark dashed line, 420 min.

material might experience a transient 6-fold increase in strain (at arbitrary position pixel 72) or 3-fold decreases in strain (at position pixels 50−60).

Over this relatively short time span, we observed small, for a polymeric material, maximum absolute axial tensile strains (∼0.3%). Strains which result from cell traction forces, however, have the potential to be fairly large. In comparison, Vanni et al. have used the pattern provided by the collagen network itself as an in situ strain gauge.[26] Over a period of 4−60 h, they observed strains in sparsely populated collagen gels (∼100−500 cells) in the range of 0.20−0.36 (20−36%). Wang et al. tracked cells on polyacrylamide gels embedded with fluorescent beads.[9] They measured displacements on this relatively stiff substrate of about 3 μm resulting from cell spreading. Our displacements, in a much more compliant medium, are on the order of 18 μm. Light scattering from metal nanoparticles, in comparison to fluorescence methods with dyes, does not suffer from photobleaching effects,[28] and fluorescence resonance energy transfer between fluorescent donors and acceptors are capable only of inferring relative positions on much smaller scales, from ∼1 to ∼10 nm, which are not as relevant for full-scale cellular motion.

Understanding the complex mechanisms involved in mechanotransduction requires methods of quantifying local mechanical effects at relevant length scales and within more realistic model systems. In particular, since it has been clearly established that cell response is significantly different in a more three-dimensional (3D) environment, as compared to flat planar substrates,[27] methods of making measurements within 3D environments are critical. Our results, demonstrated in thick films, show the potential of using gold nanorods to facilitate local deformation measurements in real time within soft tissue and ultimately in thicker gels. Our data also illustrate the capability of this technique to measure subtle strain fields within the context of a relatively large field of view, offering a method whereby multicell measurements at sub-cell-length scales can be accessed.

Other investigators have used the light elastically scattered from metal nanoparticles to detect biological molecules, to image transport processes into cells, and to infer metal nanorod rotation in solution.[28−34] On the basis of the data presented here, it is clear that the potential exists to perform these kinds of chemical studies in concert with mechanical studies, providing a more complete picture of the multiple environments experienced by living cells—all enabled by the optical properties of biocompatible metal nanoparticles.

Acknowledgment. We thank Professor Chris Robinson (USC Department of Art) for help with the figures and visualization techniques, Mary Morales (USC School of Medicine) for help with the tissue cultures, and Dr. Chris Orendorff (currently at Sandia National Laboratory) for significant scientific contributions to the above work. This work was supported by NIH Grant No. P20 RR-016461 from the National Center for Research Resources, NIH Grant No. HL73937 from the Heart, Lung and Blood Institute, and by the National Science Foundation, Grant No. CMS-0555329.

Supporting Information Available: A movie showing a fluorescence microscopy image of cells as a function of time, to show cell movement, and two movies showing the horizontal axial strains and the vertical axial strains, corresponding to the deformations shown in the first movie. This material is available free of charge via the Internet at http://pubs.acs.org.

References

(1) Humphrey, J. D. *J. Biomech. Eng., Trans. ASME* **2001**, *123*, 638−641.
(2) Roeder, B. A.; Kokini, K.; Robinson, J. P.; Voytik-Harbin, S. L. *J. Biomech. Eng., Trans. ASME* **2004**, *126*, 699−708.
(3) Costa, K. D.; Holmes, J. W.; McCulloch, A. D. *Philos. Trans. R. Soc. London, Ser. A* **2001**, *359*, 1233−1250.
(4) Grinnell, F. *Trends Cell. Biol.* **2003**, *13*, 264−269.
(5) Ingber, D. E. *Circ. Res.* **2002**, *91*, 877−887.
(6) Swartz, M. A.; Tshumperlin, D. J.; Kamm, R. D.; Drazen, J. M. *Proc. Natl. Acad. Sci. U.S.A.* **2001**, *98*, 6180−6185.
(7) Bao, G.; Suresh, S. *Nat. Mater.* **2003,** *3*, *715*−725.
(8) Zhu, C.; Bao, G.; Wang, N. *Annu. Rev. Biomed. Eng.* **2000**, *2*, 189−226.
(9) Wang, N.; Ostuni, E.; Whitesides, G. M.; Ingber, D. E. *Cell Motil. Cytoskeleton* **2002**, *52*, 97−106.
(10) Pederson, J. A.; Swatz, M. A. *Ann. Biomed. Eng.* **2005**, *33*, 1469−1490.
(11) El-Sayed, M. A. *Acc. Chem. Res.* **2001**, *34*, 257−264.
(12) *Metal Nanoparticles: Synthesis, Characterization and Applications*; Feldheim, D. L., Foss, C. A., Jr., Eds.; Marcel Dekker: New York, 2002.
(13) Kelly, K. L.; Coronado, E.; Zhao, L. L.; Schatz, G. C. *J. Phys. Chem. B* **2003**, *107*, 668−677.
(14) Sosa, I. O.; Noguez, C.; Barrera, R. G. *J. Phys. Chem. B* **2003**, *107*, 6269−6275.
(15) van der Zande, B. M. I.; Pages, L.; Hikmet, R. A. M.; van Blaaderen, A. *J. Phys. Chem. B* **1999**, *103*, 5761−5767.
(16) Orendorff, C. J.; Baxter, S. C.; Goldsmith, E. C.; Murphy, C. J. *Nanotechnology* **2005**, *16*, 2601−2605.
(17) Jana, N. R.; Gearheart, L.; Murphy, C. J. *Adv. Mater.* **2001**, *13*, 1389−1393.
(18) Jana, N. R.; Gearheart, L.; Murphy, C. J. *J. Phys. Chem. B* **2001**, *105*, 4065−4067.
(19) Murphy, C. J.; Sau, T. K.; Gole, A. M.; Orendroff, C. J.; Gao, J.; Gou, L.; Hunyadi, S. E.; Li, T. *J. Phys. Chem. B* **2005**, *109*, 13857−13870.
(20) Nikoobakht, B.; El-Sayed, M. A. *Langmuir* **2001**, *17*, 6368−6374.
(21) Sau, T. K.; Murphy, C. J. *Langmuir* **2005**, *21*, 2923−2329.
(22) Connor, E. E.; Mwamuka, J.; Gole, A.; Murphy, C. J.; Wyatt, M. D. *Small* **2005**, *1*, 325−327.
(23) Bell, E.; Ivarsson, B.; Merill, C. *Proc. Natl. Acad. Sci. U.S.A.* **1979**, *76*, 1274−1278.
(24) Birk, D.; Frederick, H.; Trelstad, R. L.; Trelstad, S. *Cell Biology of the Extracellular Matrix*, 2nd ed.; Plenum Press: New York and London, 1991; pp 221−249.
(25) Sutton, M. A.; Wolters, W. J.; Peters, W. H.; Ranson, W. F.; McNeill, S. R. *Image Vision Computing* **1983**, *1*, 133−139.
(26) Vanni, S.; Lagerholm, C.; Otey, C.; Taylor, L. D.; Lanni, F. *Biophys. J.* **2003**, *84*, 2715−2727.
(27) Pankov, C. E.; Stevens, D. R.; Yamada, K. M. *Science* **2001**, *294*, 1708−1712.
(28) Schultz, S.; Smith, D. R.; Mock, J. J.; Schultz, D. A. *Proc. Natl. Acad. Sci. U.S.A.* **2000**, *97*, 996−1001.
(29) Xu, X.-H. N.; Chen, J.; Jeffers, R. B.; Kyriacou, S. *Nano Lett.* **2002**, *2*, 175−182.
(30) McFarland, A. D.; Van Duyne, R. P. *Nano Lett.* **2003**, *3*, 1057−1062.
(31) Raschke, G.; Kowarik, S.; Franzl, T.; Sonnichsen, C.; Klar, T. A.; Feldmann, J.; Nichtl, A.; Kurzinger, K. *Nano Lett.* **2003**, *3*, 935−938.
(32) Xu, X.-H. N.; Brownlow, W. J.; Kyriacou, S. V.; Wan, Q.; Viola, J. J. *Biochemistry* **2004**, *43*, 10400−10413.
(33) El-Sayed, I. H.; Huang, X.; El-Sayed, M. A. *Nano Lett.* **2005**, *5*, 829−834.
(34) Sonnichsen, C.; Alivisatos, A. P. *Nano Lett.* **2005**, *5*, 301−304.

NL062248D